Journal of Applied Sciences 15 (4): 644-653, 2015
ISSN 1812-5654

ansinet
Asian Network for Scientific Information

RESEARCH ARTICLE OPEN ACCESS

DOI: 10.3923/jas.2015.644.653

3D Numerical Simulation of Propeller and its Aerodynamic Interference Effects on Tail of a Flying Boat

[1]Hossein Afshar and [2,3]Mohammad Ali Keshvari
[1]Department of Mechanical Engineering, East Tehran Branch, Islamic Azad University, Tehran, Iran
[2]Department of Mechanical Engineering, Tehran Science and Research Branch, Islamic Azad University, Damavand, Iran
[3]Department of Mechanical Engineering, Damavand Branch, Islamic Azad University, Damavand, Iran

ARTICLE INFO
Article History:
Received: October 03, 2014
Accepted: January 12, 2015

Corresponding Author:
Hossein Afshar,
Department of Mechanical Engineering,
East Tehran Branch,
Islamic Azad University, Tehran, Iran

ABSTRACT
In this study, considering the complexity of flow and its three dimensional nature, aerodynamic coefficients of a propeller is obtained and the effects of propeller flow on the tail were analyzed by solving Navier-Stokes equations numerically. The results indicated that the position of the propeller toward the tail has to neutralize the torque produced by the propeller as much as possible. At the same time, the lift and drag of the tail have to be in the proper range. The best angle and direction for propeller installation is proposed. Computational fluid dynamics were applied to find the flow about the propeller and the tail and to determine their interaction effects.

Key words: Propeller, aerodynamic coefficients, interference effects, computational fluid dynamics, flying boat

INTRODUCTION

Determination of the interference effects of a flying object component is crucial in designing and optimizing its complex shape. An appropriate design will require an arrangement of components that result in positive interference effects. Such effects can only be obtained by evaluating each component once alone and once in combination with other components through simple, cost-effective methods of computational fluid dynamics.

A propeller uses the engine power and creates thrust whose value is not constant for a particular propeller, i.e., it depends on the propeller's diameter, linear velocity and rotational speed. Although decreased inlet flow rate is generally associated with increased thrust, considering the definition of relative velocity, the geometry of a propeller and thus flow separation (stall) in some parts of the propeller blades, especially in those with great airfoil angles at the root, reduces the static thrust when reaching inertia. Therefore, static thrust is not an appropriate criterion for propeller assessment and the propeller is designed for maximum productivity at a certain speed.

Meanwhile, propellers with similar shape and equal form factors will display similar behaviors. Performance of propellers is assessed based on a number of dimensionless coefficients including advance ratio, power factor and thrust coefficient. Moreover, in order to evaluate the effects of the propeller on the tail, it is first necessary to somehow determine the propeller flow field.

There are many studies related to WIG's operation. Some of them are Joh and Kim (2004) numerically studied the pressure changes, drag and static height stability a round WIG craft airfoil two and three dimensional configuration. Kim *et al.* (2009) performed the optimization of the shape and the configuration of the WIG craft including fuselage, main wing, tail and side wing, The SQP (Sequential Quadratic Programming) for the optimization and the VLM (Vortex Lattice Method) for the evaluation of the flow around a WIG craft were employed. Kornev and Matveev (2003) analyzed the static height stability using the vortex lattices method. Rozhdestvensky (2006) attempts to improve the stability and controllability of a WIG effect vehicle have included employing a large horizontal tail, a tandem configuration. Afshar and Alishahi (2009) the flow field about

a complete flying-boat in ground effect is resolved. The influences of using winglet in ground and out of ground effect are compared and it is shown that ground effects this influence to a large extent. Park and Lee (2008) carried out a numerical investigation on the effect of an endplate at various angels of attack and ground clearances. They found that the end plate prevented the high pressure air form escaping out of the lower wing surface and so reduced the influence of the wing-tip vortex and further argument the lift and drag ratio. Kikuchi *et al.* (1997) measured the interaction forces on the air foil and compare their result with those of the numerical results. Yakhot *et al.* (1992) described that it's known that the RNG k-ε model with an additional term in its ε-equation can significantly improve the accuracy of turbulent flow. Chun and Chang (2002) performed the experimental study for the static and dynamic stability based on the wind tunnel test. The model vehicle was the 20-passenger WIG craft. They clearly showed the implication of the static height and dynamic stability in their study. They concluded that one of the ways in increasing the static stability and the damping ratio for the short period pitching oscillation was to increase the tail wing size. However, they pointed out that the large tail increased the structural weight and the drag. Kim and Chun (1998) performed computational optimization for an airfoil shape. They chose the pressure distributions (inverse design) and lift coefficient as the objective functions and obtained their optimal solutions using a Sequential Quadratic Programming (SQP) method which, is a gradient-based local optimization technique. Lee and Lee (2011) performed a numerical optimization on a three-dimensional wing in ground effect. They classified four different groups of pure to individuals according to the wing configuration: The drag and static height stability group, the lift group and the intermediate group. Hirata and Hino (1997) conducted a numerical investigation on Power Augmented Ram (PAR) wing in ground effect, considering two boundary conditions: (1) A moving belt ground plate condition and (2) A fixed ground plate condition corresponding to a wind tunnel test. Murao *et al.* (2005) stated that two ducted propellers were installed before the wing. The lift force is increased by 50% as compared to that without PAR. Wind tunnel performance of a WIG craft with Propeller-Deflected Slipstream (PDS). In calculating aerodynamic forces on lifting surfaces of WIG craft in cruising flight regimes, the water surface deformations are usually minimal and neglected (Barber *et al.*, 1998; Masuda and Suzuki, 1991). In calculating aerodynamic forces on lifting surfaces of WIG craft in cruising flight regimes, the water surface deformations are usually minimal and neglected. Later Molina and Zhang (2011) described when the airfoil is in close proximity to the ground, the flows are dominated by the viscous effects at the low reduced frequencies, whereas the inviscid flow behaviors are acceptable at the high reduced frequencies. Tuck (1984) the water surface deformations can become significant and change the effective dimensions of the channel between the wing and water, thus affecting the aerodynamic forces. For steady analysis of this flow with water surface deformations, a hydrostatic assumption the water surface depression (Ellington *et al.*, 1996) via a classical linear theory about a vertically oscillating wing in the inviscid flow.

METHODOLOGY

Geometry of the propeller: An airplane propeller with 10 ft diameter and a fixed pitch of 7 ft was selected to assess the effects of propeller on tail. The physical and aerodynamic twist of the propeller and it's taper from root to tip is shown in Fig. 1. The propeller is divided into subsections for structured grid generation as O type for each blade and H type for the space between two blades.

The airfoils are also presented at different radius in Fig. 2. The dimensions of all figures are expressed in mm.

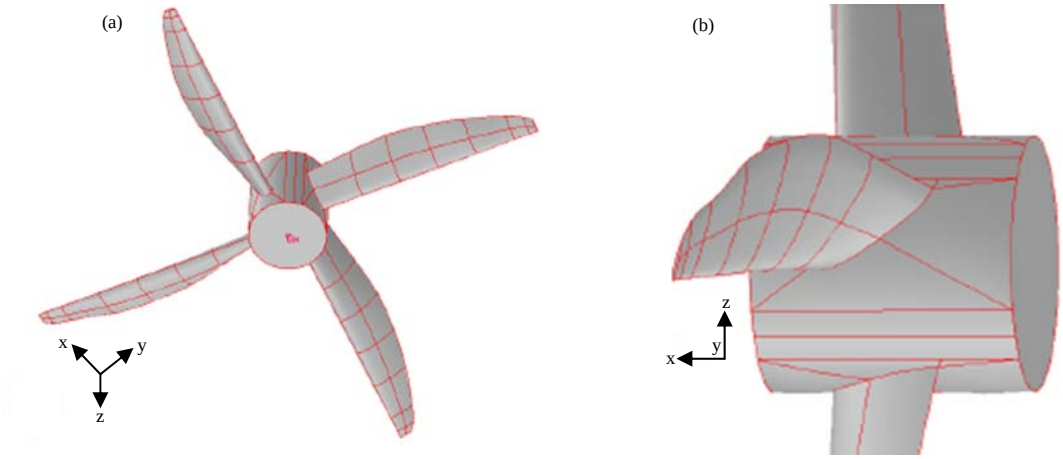

Fig. 1(a-b): Physical and aerodynamic twist of the propellers

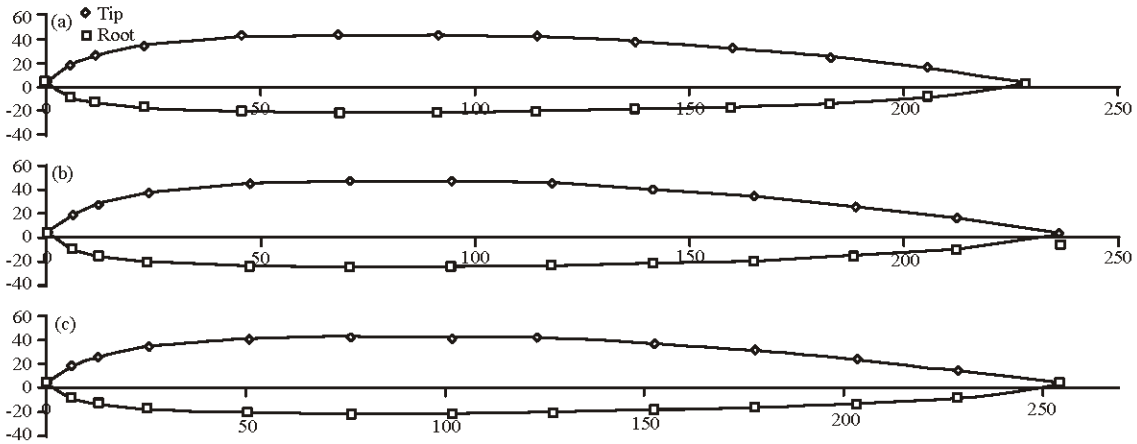

Fig. 2(a-c): Dimensions of airfoils, (a) r/R = 0.15, (b) r/R = 0.3 and (c) r/R = 0.45

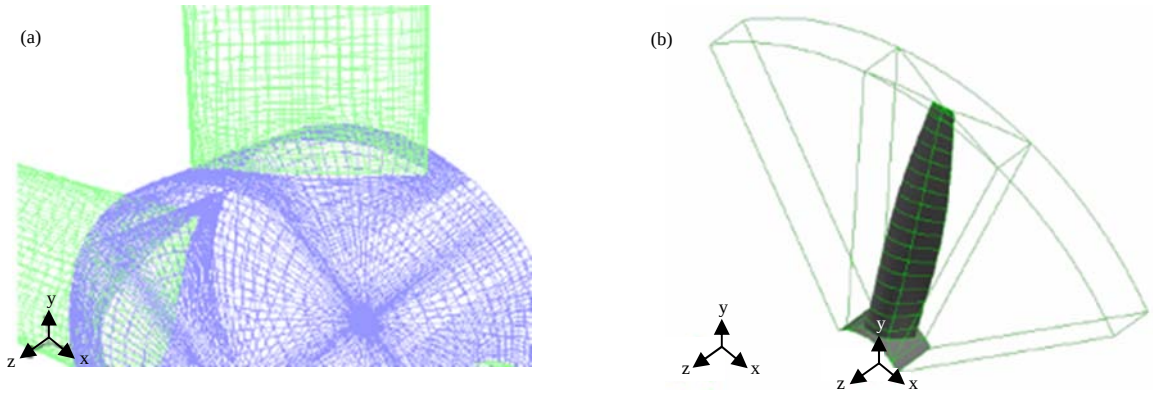

Fig. 3(a-b): Grid generation around the propeller

The airfoil installation angle is 56 and 12.5° at root and tip, respectively. Besides, its chord is 228.5 and 67.5 mm at root and tip, respectively.

Grid generation around the propeller: Physical and aerodynamic twist of the blades and varying chord and thickness of the airfoil from the root to the tip complicate the process of grid generating around the propeller. Hence, after testing all possible grids, a structured grid comprising O and H grids (with some unstructured parts) was created. As shown in Fig. 3, the O and H grids were used around each blade and between two blades, respectively. Grids on the front and rear plates of the hub and on the tips were unstructured. Grids on the front and rear plates (a little before and after the propeller) were in the form of O type.

Governing equations: Since the Mach number of boat speed was less than 0.3, the flow was considered to be incompressible. The Reynolds number was computed at about 10 and the flow was thus turbulent. The terms resulting from turbulence in the transport equation were modeled with the k-ε turbulence model. Non-temporal governing equations were as follows.

The continuity equation:

$$\frac{\partial u}{\partial x}+\frac{\partial \upsilon}{\partial y}+\frac{\partial \omega}{\partial z}=0$$

Navier-Stokes equation in the inertial frame:

$$\rho\nabla.(\vec{\upsilon}.\vec{\upsilon})=-\nabla p+\nabla.(\bar{\bar{\tau}})$$

Navier-Stokes equation in the rotating frame with absolute velocity:

$$\nabla.(\rho\vec{\upsilon}_r\vec{\upsilon})+\vec{\Omega}\times\vec{\upsilon}=-\nabla_p+\nabla.\bar{\bar{\tau}}$$

where, u, υ and ω are the components of velocity along the x, y and z axes, respectively. Moreover, τ_{ij} is the components of stress tensor and is defined as:

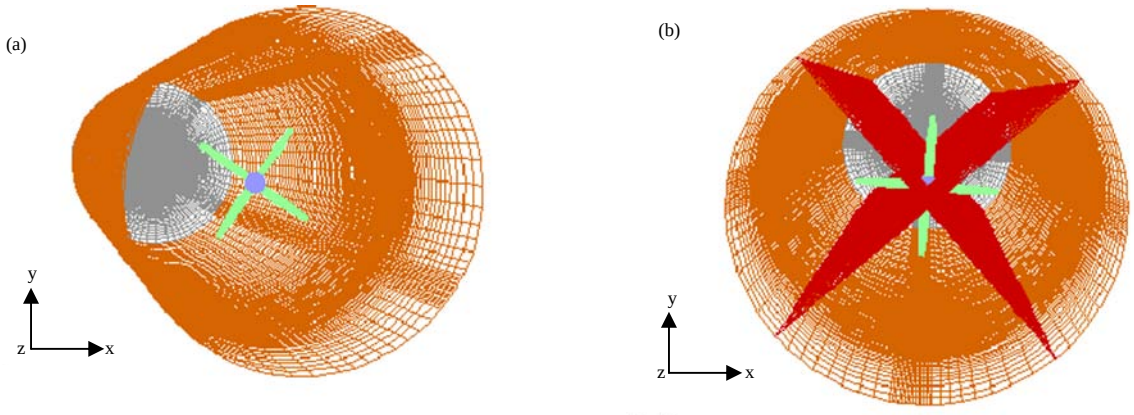

Fig. 4(a-b): Propellers in rotating coordinate system

$$\bar{\bar{\tau}} = (\mu + \mu T)\left[(\nabla\vec{\upsilon} + \nabla\vec{\upsilon}^{T}) - \frac{2}{3}\nabla.\vec{\upsilon}I\right]$$

where, $\vec{\upsilon}$ is the velocity vector and I is the unit tensor.

The k-ε equations:

$$\rho\frac{\partial}{\partial_{xi}}(k\upsilon_i) = \frac{\partial}{\partial_{xj}}\left[\left(\mu + \frac{\mu_t}{\sigma_k}\right)\frac{\partial_k}{\partial_{xj}}\right] + G - \rho\varepsilon$$

$$\rho\frac{\partial}{\partial x_i}(\varepsilon u_i) = \frac{\partial}{\partial x_j}\left[\left(\mu + \frac{\mu_t}{\sigma_\varepsilon}\right)\frac{\partial_\varepsilon}{\partial x_j}\right] + C_1\frac{\varepsilon}{k}G - C_2\rho\frac{\varepsilon^2}{k}$$

$$\mu_t = \rho C_\mu\frac{k^2}{\varepsilon}$$

where, C_1 and C_2 are empirical coefficients and σ_ε and σ_k are the turbulent Schmidt and Prandtl numbers:

$$C_1 = 1.44,\ C_2 = 1.92,\ C_\mu = 0.09,\ \sigma_k = 1,\ \sigma_\varepsilon = 1.3$$

Boundary conditions: The boat's speed and the propeller's angular velocity are considered as 30 m sec^{-1} and 237 rad sec^{-1}, respectively. The rotational flow produced by the propeller-a temporal flow that depends on the number of blades (n = 4 in this study)-destroys the symmetry.

Considering the propeller inflow and tip Mach numbers (<0.3 and about 0.62, respectively), the flow is compressible at the tips. Nevertheless as the region of compressible flow is too small compared to the evaluated domain, the flow was assumed to be incompressible and the equations were thus elliptic. Supposing the air to move toward the object, the velocity was set at the front, side, bottom and top plates as boundary condition. At the output plate, however, the boundary condition was determined as the pressure. A no slip condition was also adopted on the blades and at the horizontal and vertical tails. Knowing that only the propeller rotates and other parts are fixed, the air around the propeller is separated from the rest of the domain and the flow equations in this region are solved in a rotating coordinate system.

Solution: The computational domain for obtaining aerodynamic characteristics of the propeller is shown in Fig. 4. Finite-volume method was used to solve the governing equations. The SIMPLE algorithm with first-order accuracy was applied to couple velocity and pressure. Momentum and flow-related equations were solved using a first-order upwind scheme. Turbulence was modeled with the standard k-ε turbulence model.

The volumes around the objects were assessed in grids containing 6×10^5, 1.55×10^6, 2.1×10^6 and 3.0×10^6 cells. While the results from the first two grids had substantial differences, the two latter grids were slightly different. In fact, using the k-ε turbulence model has moved the nodes in the three-million cell grid toward the object's borders and placed y+between 30 and 60. Consequently, this grid was used in calculating the aerodynamic coefficients.

RESULTS

Pressure distribution along the propeller and the hub: Figure 5 and 6 demonstrate the pressure counters on the propeller blades and the hub. Maximum pressure was toward the leading edge and the rear part but dramatically reduced thereafter.

The pressure was maximum at the tip but decreased and so did the thrust, along the blade to the root. Changes in pressure on the hub were smaller than those on the tip. Hence, the hub has to be evaluated alone if pressure distribution is to be shown. Pressure distribution on the hub is shown in Fig. 7.

As the Fig. 7 depicts the cross-section of the airfoils on the hub, pressure was high in the back of the propeller and low on the airfoil, i.e., a driving force in the positive direction of the x-axis was expected.

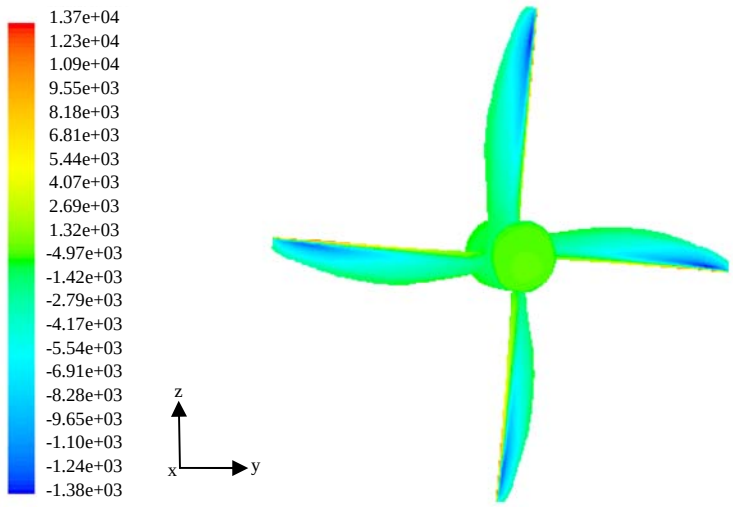

Fig. 5: Pressure distribution on the front face of the propeller

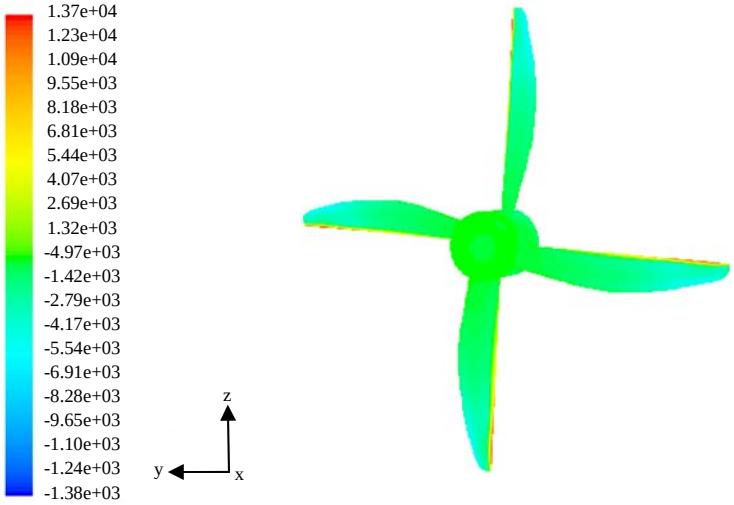

Fig. 6: Pressure distribution on the rear face of the propeller

Pressure distribution on the tail: Pressure distribution on the tail was assessed in three states:

- There was no angle between the propeller and the junction of the two tails
- The propeller was 7° below and 2.5° to the left of the junction of the two tails and the boat moved in the direction of the propeller
- The propeller was 7° below and 2.5° to the left of the junction of the two tails and the boat moved in the direction of the tail

In the first state, none of the propeller and the tail was in the angle of attack. In the second state, the propeller was not at the angle of attack but the tail was. In the third state, however, the propeller was at the angle of attack but the tail was not.

The x-axis was along the longitudinal direction of the flying boat from the end to the nose. The z-axis was upward and the y-axis pointed to the left when standing in the direction of the x-axis. The propeller rotated in the negative direction of the x-axis. Hereafter, left and right are defined based on the positive direction of the x-axis. Since the propeller turned counterclockwise (a left handed propeller), the vortex caused by the propeller hit the top and left surfaces of the horizontal tail, the left surface of the vertical tail and the bottom and right surfaces of the horizontal tail and thus increased the pressure at these areas. Figure 8 shows the pressure distribution counter when the propeller had no angle with the junction of the two tails.

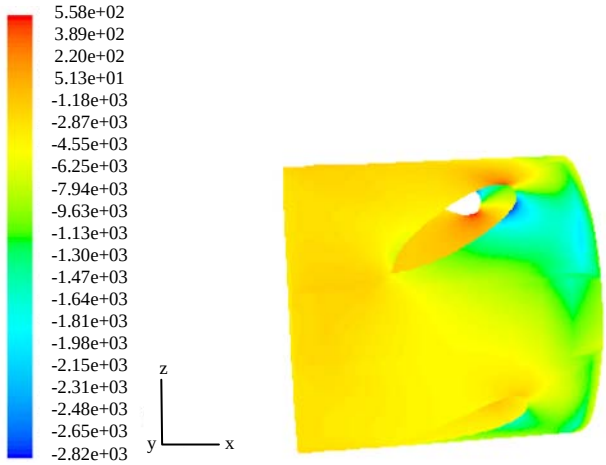

Fig. 7: Pressure distribution on the hub

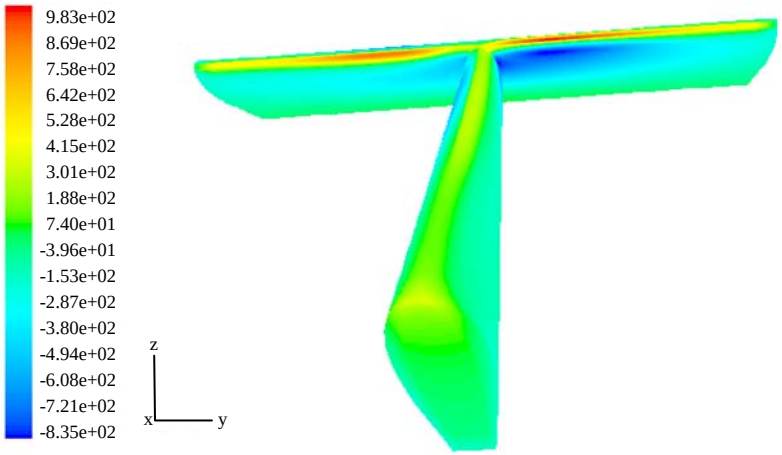

Fig. 8: Pressure distribution counter when the propeller had no angle with the junction of the two tails

This pressure distribution would produce a torsional moment in the negative direction of the x-axis and also in the positive direction of the z-axis in the operating conditions of the propeller. Such a situation would create the yaw moment which can be neutralized by turning the propeller in a way that its axial flow hits the right side of the vertical tail. This justifies the 2.5° diversion of the propeller.

Figure 9 shows pressure distribution on top and bottom surfaces of the horizontal tail.

Evidently, maximum pressure was imposed on the right leading edge of the horizontal tail and the pressure distribution on the leading edge was completely non-uniform.

Figure 10 shows pressure distribution on the tail when the propeller made an angle with it and the boat moved in the direction of the tail.

As it is seen, the propeller shaft has diverted downward. It can thus be concluded that the vortex caused by the propeller has had the least contact with the horizontal tail. Therefore, the minimum pressure underneath the horizontal tail has increased compared to the conditions when propeller shaft was not diverted.

Velocity distribution: Velocity distribution at different parts of the solution domain was studied when the propeller and the tail made an angle and the boat was moving in the direction of the tail.

Figure 11 demonstrates velocity vectors along the propeller blades.

Considering the small turning radius near the root, the tangential velocity of the flow was also small at this area. As the angle between the chord line and the airfoil at the root was

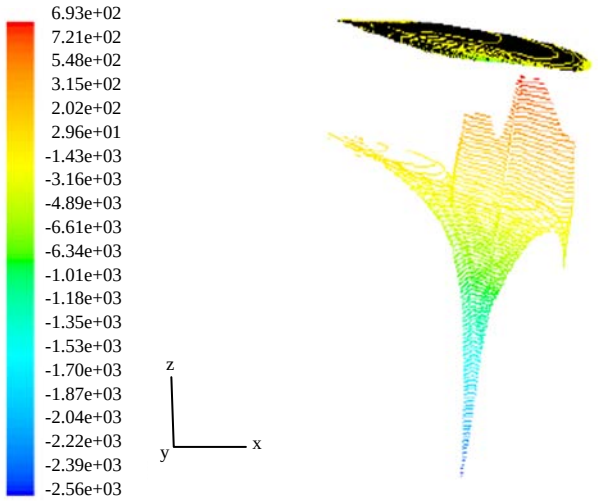

Fig. 9: Pressure distribution on top and bottom surfaces of the horizontal tail

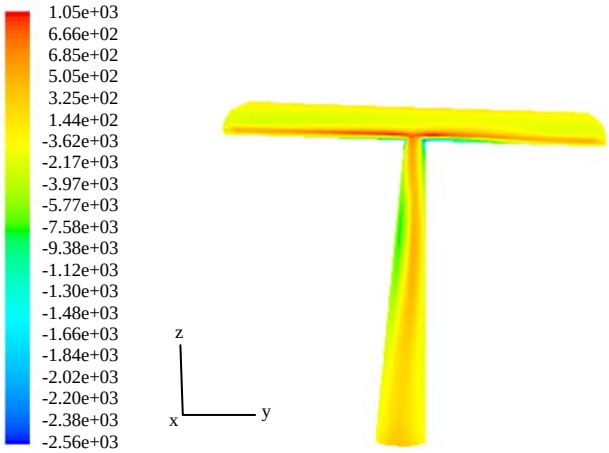

Fig. 10: Pressure distribution on the tail when the propeller made an angle with tail

about 56°, the angle of attack caused by the relative wind was a high, negative value at the root. In other words as the Fig. 10 displays, the flow separated near the root and an adverse pressure gradient occurred. Due to the vortexes produced at the tip, maximum velocity was detected at a radius equal to 0.75 of the propeller radius. The obtained maximum velocity (122 m sec^{-1}) and Mach number (0.37) under such conditions prove the assumption of incompressible flow to be true.

Figure 12 shows the axial velocity distribution on the propeller plate.

Apparently, the axial velocity distribution on the propeller was absolutely uniform. On the blades, however, it was substantially great compared to the distance between two blades. In addition, axial velocity on each blade decreased from the tip to the root.

DISCUSSION

The thrust of the propeller under static operating conditions is measured and it is compared with numerical results. The comparison for different operating conditions is shown in Table 1.

In all conditions, the measured thrust is higher than the calculated one. As a fixed-pitch propeller was studied, the angle of airfoils at different cross-sections could be measured which is summarized in Table 2. These values were compared with those obtained from the AutoCAD model.

Apparently, the error was higher near the root. Under static conditions and low rotation, the thrust is predominantly generated by the airfoils close to the root.

Forces applied to the tail and propellers under various conditions are summarized in Table 3.

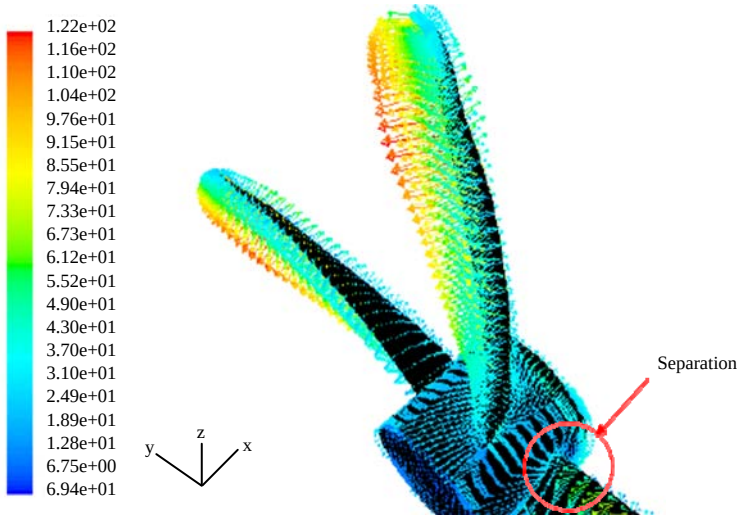

Fig. 11: Velocity vectors along the propeller blades

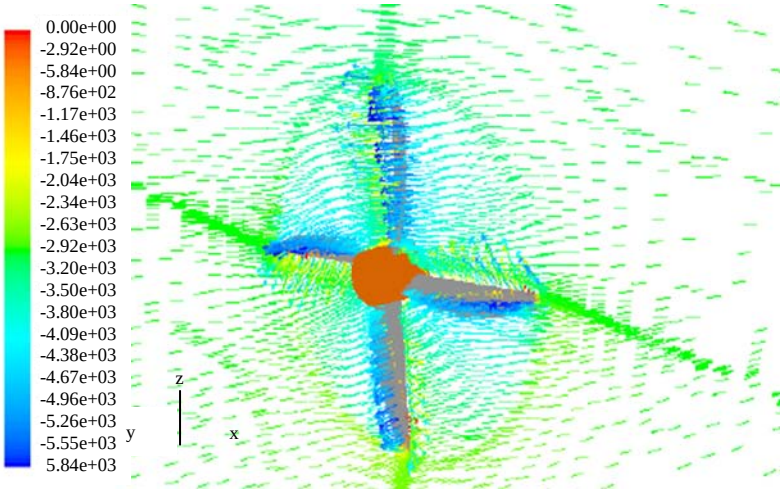

Fig. 12: Axial velocity distribution on the propeller plate

Table 1: Measured thrust of the propeller, J = v/n.D

Propeller-fix pitch = 58

n (rpm)	n (rad sec^{-1})	D (m)	V (m sec^{-1})	J	Thrust (kg)	Thrust (kg) (Experiment)	Error (%)
1200	51.71	1.62	0.1	0.0075	9.387755102	29	67.628
3000	129.28	1.62	0.1	0.003	59.02040816	70	15.685
4000	172.38	1.62	0.1	0.00225	105.1020408	110	4.4527
5000	215.47	1.62	0.1	0.0018	164.1959184	182	9.7825
5200	224.10	1.62	0.1	0.001730769	177.8448980	192	7.3724
5500	237.00	1.62	0.1	0.001636364	198.7387755	230	13.592

Table 2: Parameters of the propeller

r/R	Blade angle according to pitch = 58”	Measure blade angle in AutoCAD	Error (%)
0.192	55.69042639	37.40	32.843
0.308	42.37492325	34.20	19.292
0.423	33.59261509	30.00	10.695
0.538	27.57348956	26.10	5.3439
0.654	23.23998459	22.60	2.7538
0.75	20.53333816	20.20	1.6234
0.769	20.06287557	19.70	1.8087
0.884	17.62536715	16.02	8.0870

Table 3: Forces applied to the tail and propellers

Parameters	Thrust (N)	Mx (N.M)	Lift (N)	Drag (N) All drag numbers are positive	Perpendicular force to the horizontal tail for Y	M (V.H tail cross) (N.M)		
At FSV: 30 m sec^{-1}, PAV: 237 rad sec^{-1} and AAPT: 0°								
Propeller	606.15	285.16						
Propeller and tail with aerodynamic interferences effect	610.73	285.84	-68.03	-101.34	-125.28	-240.28	33.13	-162.06
At FSV: 30 m sec^{-1} and PAV: 0 rad sec^{-1}								
Propeller and tail with aerodynamic interferences effect	-243		-23.71	-87.88	30.14	48.49	36.98	36.24
At FSV: 30 m sec^{-1}, PAV: 237 rad sec^{-1} and Propeller position*								
Propeller and tail with aerodynamic interferences effect	626.77	287.36	-559.08	174.28	-131.94			
At FSV: 30 m sec^{-1}, PAV: 237 rad sec^{-1} and Propeller position**								
Propeller and tail with aerodynamic interferences effect	612.66	286.12	1037.05	-216.566	218.0075			

FSV: Free stream velocity, PAV: Propeller angular velocity, AAPT: Angle of attack of propeller and tail, *Propeller has 7 degrees towards down, relative to intersection point of two tails and 2.5° towards left and movement of boat is towards propeller and **Propeller has 7 degrees towards down relative to intersection point of two tails and 2.5° towards left and movement direction of boat is towards tail

Drag of a typical flying boat which is investigated by Afshar and Alishahi (2009) is in the range of the present propeller thrust at 5500 rpm. So this propeller with the suggested installing condition can be used to power the flying boat.

CONCLUSION

Turning the propeller shaft 7° downward and 2.5° toward the negative direction of the z-axis when the boat is moving in the direction of the tail will place the propeller at the angle of attack. Since the angle of attack of the tail is zero in this situation, its drag will increase by 50%. In fact, even when the installation angle of the propeller is zero and the tail is at the angle of attack with the axial velocity component of the propeller flow, the angle of attack of the tail will not be zero due to the vortex produced by the propeller. Meanwhile, dramatic increase of the angle of attack in the second situation will definitely increase the torque about the z-axis.

When the boat moves in the direction of propeller shaft (which is generally the case since the thrust of the propeller as the only propulsion power of the flying boat, is in the direction of the propeller shaft), the applied negative lift force on the tail would be 14 times higher compared to the previous conditions. This state is appropriate for adjustments. Under such conditions, the torque would be negative and 70% less in value compared to the previous state. Therefore, turning the propeller by less than 2.5° will not only neutralize the torque but also reduce the boat's deviation from the x-axis.

The presented results show that the static balancing of a flying boat cannot guarantee its stability and there are restrict limitations in this regard. Considering the aerodynamic interaction of propeller with parts of a flying boat is mandatory in assembling the parts.

REFERENCES

Afshar, H. and M.M. Alishahi, 2009. A study of winglet and aerodynamics interference in 3-D viscous flow around a flying-boat in ground effect. J. Applied Sci., 9: 3752-3757.

Barber, T., E. Leonardi and D. Archer, 1998. Free surface deformation caused by a wing in ground effect over water. Proceedings of the International Workshop on WISE Up to Ekranoplan GEMs, June 15-16, 1998, The University of New South Wales, Sydney, Australia.

Chun, H.H. and C.H. Chang, 2002. Longitudinal stability and dynamic motions of a small passenger WIG craft. Ocean Eng., 29: 1145-1162.

Ellington, C.P., C. van den Berg, A.P. Willmott and A.L.R. Thomas, 1996. Leading-edge vortices in insect flight. Nature, 384: 626-630.

Hirata, N. and T. Hino, 1997. Investigation of a three-dimensional power-augmented ram wing in ground effect. Proceedings of 35th Aerospace Sciences Meeting and Exhibition, January 6-9, 1997, Reno, Nevada.

Joh, C.Y. and Y.J. Kim, 2004. [Computational aerodynamic analysis of airfoils for WIG (airfoil-in-ground-effect)-craft]. J. Korean Soc. Aeronaut. Space Sci., 32: 37-46, (In Korean).

Kikuchi, K., F. Motoe and M. Yanagizawa, 1997. Numerical simulation of the ground effect using the boundary element method. Int. J. Numer. Methods Fluids, 25: 1043-1056.

Kim, H.J. and H.H. Chun, 1998. Design of 2-dimensional WIG section by a nonlinear optimization method. J. Soc. Naval Archit. Korea, 35: 50-59.

Kim, H.J., H.H. Chun and K.H. Jung, 2009. Aeronumeric optimal design of a wing-in-ground-effect craft. J. Mar. Sci. Technol., 14: 39-50.

Kornev, N. and K. Matveev, 2003. Complex numerical modeling of dynamics and crashes of wing-in-ground vehicles. Proceedings of the 41st AIAA Aerospace Sciences Meeting and Exhibition, January 6-9, 2003, Reno, Nevada.

Lee, S.H. and J. Lee, 2011. Optimization of three-dimensional wings in ground effect using multiobjective genetic algorithm. J. Aircraft, 48: 1633-1645.

Masuda, S. and K. Suzuki, 1991. Simulation of hydrodynamic effects of 2-dimensional WIG moving near the free surface. J. Soc. Naval Archit. Jpn., 170: 83-92.

Molina, J. and X. Zhang, 2011. Aerodynamics of a heaving airfoil in ground effect. AIAA J., 49: 1168-1179.

Murao, R., S. Seki and N. Tomita, 2005. On a study of a WIG with Propeller-Deflected Slipstream (PDS) by using a radio controlled model. Proceedings of the 8th International Conference on Fast Sea Transportation, June 27-30, 2005, Saint-Petersburg, Russia.

Park, K. and J. Lee, 2008. Influence of endplate on aerodynamic characteristics of low-aspect-ratio wing in ground effect. J. Mech. Sci. Technol., 22: 2578-2589.

Rozhdestvensky, K.V., 2006. Wing-in-ground effect vehicles. Prog. Aerospace Sci., 42: 211-283.

Tuck, E.O., 1984. A simple one-dimensional theory for air-supported vehicles over water. J. Ship Res., 28: 290-292.

Yakhot, V., S.A. Orszag, S. Thangam, T.B. Gatski and C.G. Speziale, 1992. Development of turbulence models for shear flows by a double expansion technique. Phys. Fluids A, 4: 1510-1520.